A calibration procedure for a traceable contamination analysis on medical devices by combined X-ray spectrometry and ambient spectroscopic techniques

A calibration procedure for a reliable contamination analysis on medical devices by combined X-ray spectrometry and ambient spectroscopic techniques

Beatrix Pollakowski-Herrmann,*[†] Andrea Hornemann, [†] Andrea M Giovannozzi,[$] Felicia Green, [‡] Paul Gunning, [‖] Chiara Portesi, [$] Andrea Rossi, [$] Christian Seim, [†] Rory Steven, [‡] Bonnie Tyler, [‡,§] and Burkhard Beckhoff[†]

[†]*Physikalisch-Technische Bundesanstalt (PTB), Abbestr. 2-12, 10587 Berlin, Germany,*

[$] *Quality of Life Division, INRIM, Strada delle Cacce 91, 10135 Torino, Italy,*

[‡]*National Physical Laboratory, Hampton Road, Teddington TW11 0LW, United Kingdom,*

[§]*present adress: Westfälische Wilhelms-Universität Münster Schlossplatz 2, 48149 Münster, Germany,*

[‖]*Smith & Nephew, 101 Hessle Road, Hull, HU3 2BN, United Kingdom,*

*Author for correspondence:

Dr. rer. nat. Beatrix Pollakowski-Herrmann
Mail: beatrix.pollakowski@ptb.de
Phone: +49 30 3481 7177
Fax: +49 30 3481 7103

Abstract

There is a strong need in medical device industry to decrease failure rates of biomedical devices by the reduction of defect structures and contaminants during the production process. Reliable detection and identification of defect structures and contaminants is a crucial aspect

for many industrial applications. The present study aims to provide an analytical tool for the reliable and traceable characterization of surface contaminants of medical devices, in particular N,N'-ethylene-bis (stearamide), an ubiquitous compound used in many industrial applications as a release agent or friction reduction additive.

Reference-free X-ray fluorescence analysis as primary method has proven to being able to lay foundation for all other applied methods since it yields the absolute mass deposition of the selected N,N'-ethylene-bis (stearamide) contaminant whilst X-ray absorption fine structure analysis confirms the chemical species. Ambient vibrational and mass spectroscopic methodologies such as Fourier transform infrared, Raman, and secondary ion mass spectroscopy is involved in this systematic procedure for an extensive complementary analysis.

This calibration procedure was developed using specially designed and fabricated model systems varying in thickness and substrate material. Furthermore, typical real medical devices such as both a polyethylene hip liner and a silver-coated wound dressing have been contaminated and investigated by these diverse methods, enabling validation of this developed procedure. These well-characterized specimens may be used as calibration standards for bench top instrumentation in view of a reliable and traceable analysis of biomaterials and surface treatments. These findings demonstrate the potential of combining complementary methods for a better understanding of the relevant organic materials.

1. Introduction.

Medical devices regulation necessitates for the most reliable identification and characterization methodology, providing robust measurands on failure rates, contaminants amounts and defect structures, ensuring quality control during industrial production. If enough appropriate calibration samples, i.e. by having a spatial and compositional structure as closed

as possible to the 'real' sample of interest, are available, most analytical techniques can provide quantitative results. When dealing with advanced biomedical devices suitable calibration samples are often lacking, as complex organic structures are required. Methods based upon physical traceability can overcome these restrictions.

Many surface characterization approaches have been applied to biomedical devices, ranging from photoelectron spectroscopy, contact angle measurements, to nanoscopical techniques [1,2], and mass spectroscopic techniques such as Time-of-flight secondary ion mass spectrometry (TOF-SIMS). Also Fourier transformed infrared (FTIR), and Raman spectroscopy are used for characterization of bulk objects, beyond the surface at a near-surface range. However, for quantification, these methods either rely on reference materials or calibration samples which are barely available for 'real' biomedical devices. For a robust analysis on medical devices an increased effort to ensure traceability and reliability needs to be made.

We present here a calibration procedure based on an absolute method on which the above mentioned techniques refer to, requiring suitable calibration samples and appropriate reference materials. By contrast, the vacuum-based technique reference-free X-ray fluorescence analysis (XRF) allows for a quantitative analysis of the elemental mass deposition, related thickness, and composition of compounds without requiring any reference materials or calibration samples.

Our Synchrotron radiation (SR)-based XRF approach uses only atomic fundamental parameters and calibrated instrumentation, thus enabling quantitative analysis. To ensure that the ascertained mass deposition closely relates to the assumed chemical species, Near-edge X-ray absorption fine structure spectroscopy (NEXAFS) is additionally employed to identify the chemical binding state of the sample and to confirm chemical identification. Established methods such as FTIR, Raman, and mass spectrometry are also applied for comparing the results of all measurement strategies with respect to chemical speciation. Particularly, these

techniques are qualified to deliver quantitative results through correlation with results obtained by X-ray spectroscopic techniques. It has to be noted here that both vibrational spectroscopic methods also provide information about the chemical binding state of organic compounds by so-called molecular fingerprints, enabling their distinct identification.

For the development of such a calibration procedure, 'model systems' such as organic surface contaminant layers with a dedicated thicknesses and chemical binding state were deposited onto different biomedically relevant substrates, namely polyethylene (HDPE), and silicon (Si). The organic compound N,N'-ethylene-bis (stearamide), referred to as stearamide or EBS from here onwards, has been chosen as a typical contamination. Stearamide is an ubiquitous component being used in many industrial applications as a release agent or friction reduction additive [3]. It is a small molecule waxy material that can migrate through polymers and produce surface blooms which is perfectly desirable for release functionality during the manufacture of various components, films, membranes, etc. However, in the EU and other jurisdictions stearamide is classified as an irritant compound [3] and is therefore undesirable on medical devices, particularly in cases in which the products may get in contact with skin or internal tissues [3]. Surface blooms of stearamide can also hamper fabrication of multi-component products, increasing the risk of failures of adhesive bonding, welds or laminations [3]. Stearamide blooms can also affect finished products, packaging or the processability of raw materials during manufacture [3]. Wound dressings and replacement joint prostheses represent examples of two medical device types that are usually in contact with body fluids and tissue, so any surface blooms of stearamide have to be avoided in terms of biocompatibility.

Model surface-contaminant layers comprising N,N'-ethylene-bis (stearamide) of different thicknesses were analyzed with XRF, Raman, and FTIR. The XRF intensity related thickness can be correlated with stearamide-related vibrational spectroscopic band integrals as a

calibration relationship for Raman and FTIR. It should be noted here that these well-qualified model samples may be used also as calibration samples for bench top instrumentation in laboratories in view of a reliable and traceable analysis of complex biomedical devices that are either contaminated with an unknown amount or exposed to different types of surface treatments during industrial manufacturing. Addressing analytical requirements of industry, biomedical devices such as a polyethylene-based hip liner and a silver-coated wound dressing that have been contaminated with stearamide were analyzed by XRF, Raman and FTIR spectroscopy applying the new calibration procedure based on physical traceability.

In particular, the mass deposition of the main elements C, N and O has been determined by a fundamental parameter-based reference-free XRF technique [4]. This allows a conclusion of the elemental composition and the layer-thicknesses. These results partially confirm the nominal values deduced by the preparation process. Additionally, the respective elemental mass deposition is correlated with the chemical binding state of the elements. Typical fine structure features have been identified in the C, N and O K near-edge regions, confirming the chemical structure of stearamide. These results could also be verified by FTIR, and Raman spectroscopy, and correspondingly clearly demonstrate the potential of combining complementary methods for a better understanding of the relevant complex organic layered structures.

2. Materials and methods.

2.1. Sample preparation.

Stearamide with layer thicknesses of nominally 600 nm, 100 nm, 50 nm, and 10 nm, have been prepared onto Si, and HDPE substrates. For the coated Si substrates, precise measurements of the stearamide coating thicknesses produced were made using a Woollam M-2000DI ellipsometer, details of which are given in Appendix A. An Edwards's AUTO 306 vacuum-coater to evaporate stearamide onto the different substrate types was applied.

Stearamide has a nominal mass of 352.590 Da but it can be found with different chain lengths (cf. Figure 1). The empirical formula is $[N_2O_2C_4H_8](CH_2)_{2n}$. SIMS detected the molecular ions of the stearamide coatings with chain lengths n = 15, 16 and 17, showing no damage of the stearamide during evaporation. An uniform film across the sample with a homogenous coverage of the stearamide could be confirmed by SIMS.

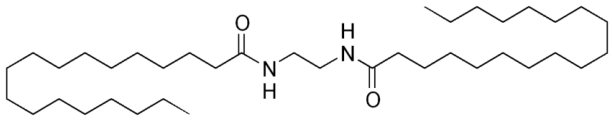

Figure 1. Molecular structure of stearamide.

In addition to the model systems stearamide was prepared on 'real' biomedical devices such as HDPE-based hip liners and silver-coated polyurethane-based wound dressings (average Ag-thickness ~ 15 µm). Both commercially available devices were provided by the company Smith and Nephew. The nominal thickness of the stearamide coatings was about 100 nm.

2.2. Reference-free XRF and X-ray absorption fine structure spectroscopy.

For analyses, the Plane Grating Monochromator (PGM) beamline for undulator radiation at the PTB laboratory at BESSY II was employed [5–7]. The beamline PGM-U49 provides monochromatized undulator radiation in the energy range from 78 eV to 1870 eV with a high spectral purity and well-known flux [5,6]. The experiments were carried out in an ultra-high vacuum chamber attached to the beamline PGM-U49. The chamber is equipped with a 9 axis manipulator, which enables a very precise sample adjustment and positioning, in particular for the incidence angle [8]. This UHV chamber, and, notably, the sample holder are placed in the focal plane of the PGM-U49, which has a vertical size of about 170 µm. The emitted fluorescence radiation from the sample is detected by a radiometrically calibrated energy-

dispersive Silicon drift detector (SDD) [6]. Both, the detector's efficiency as well as its response functions are well-known [4].

For stearamide, an optimized experimental setup has to be evaluated. Here, the conventional 45°/45° geometry is suitable for a reliable analysis of the mass-per-unit area (mass deposition). In this case, both the incidence and detection angle are about 45°. The incidence photon energy for the XRF is set to 1060 eV to excite Kα fluorescence radiation of carbon, nitrogen, and oxygen. For the NEXAFS measurements the incident photon energy is tuned in a range which is around the x-ray absorption edge to analyze chemical binding state of the respective element. Here, the C-K, N-K, and O-K absorption edges were evaluated. In fluorescence detection mode a XRF spectrum is recorded at each energy step and the fluorescence line of the element of interest is evaluated, as its deconvoluted count rate is dependent on the photon energy.

The quantitative analysis of the absolute mass m per unit area F m_i/F_I and the elemental composition are carried out by using a fundamental parameter approach as introduced in Beckhoff et al. [4]. Here, all experimental and atomic fundamental parameters have to be well-known. For this purpose, the calibrated instrumentation described in the paragraph above is used. The atomic fundamental parameters are taken from databases, e.g. Elam database [9]. Excluding the photoelectric cross section it follows from the Ebel database [10] and the fluorescence yield for the carbon K edge [11].

2.3. SR-based FTIR microspectroscopy and Raman analysis.

SR-based FTIR microspectroscopic measurements on different EBS layers on Si and HDPE substrates were performed at the IR beamline of the electron storage ring Metrology Light Source (MLS) [12–14] in the mid-infrared (MIR) spectral window from 3900 cm^{-1} to 900 cm^{-1}, using a Vertex 80v spectrometer (Bruker Optics GmbH) to which a Hyperion 3000

microscope was coupled. The spectrometer was fitted with a KBr beamsplitter. The radiation source (σ_x= 678 µm, σ_y= 245 µm) was focused through an attenuated total reflection (ATR 15×) objective onto the sample films. For single-point ATR-measurements (10 spectra per sample) a Mercury Cadmium telluride (MCT) detector was used by accumulating 512 averaged scans in reflection geometry at a beam current up to 170 mA. Background scans were collected before each sample measurement from a region free of sample material. A clean low-e-slide (Kevley Technologies) was used as a reference and rationed against the sample spectrum. All interferograms scans were submitted to a Blackman Harris 3-term window function and to a zerofilling factor of 2 prior Fourier-transformation. The sample stage compartment was thoroughly purged with dried pure gaseous nitrogen to eliminate water vapor and carbon dioxide.

Raman spectra were recorded using a Thermo Scientific DXR spectrometer equipped with a microscope, an excitation laser source at 455 nm, a motorized stage sample holder, and a charge-coupled device (CCD) detector. Spectra of stearamide samples on Si substrates were collected using a 100× microscope objective with a 10 mW laser power, a 50 µm pinhole aperture and a spectral range from 3500 to 800 cm^{-1} with a grating resolution of 5 cm^{-1}. The acquisition time was 60 s with a 5 s exposure time. Spectra of EBS samples on HDPE substrate were collected using a 100x microscope objective with an excitation laser source at 455 nm, a 10 mW laser power, a 50 µm pinhole aperture and a spectral range from 3500 to 100 cm^{-1} with a grating resolution of 5 cm^{-1}. The acquisition time was 60 s with a 5 s exposure time. The calculated laser spot size using a 455 nm laser line is about 0.68 μm^2. FTIR spectra were collected with the Opus software v.7.2 (Bruker Optics GmbH). The spectral datasets derived from ATR measurements (10 spectra) for each sample system were processed in Origin 8G (OriginLab Corporation, USA) for polynomial baseline-correction. Concerning the EBS on HDPE spectra, the NH stretching mode at 3300 cm^{-1} was fitted with a nonlinear fitting routine (Gaussian mode) for the calculation of band integrals. Raman spectra

were collected with the Omnic software v.8.1 (Thermo Fisher Scientific Inc.). At least 20 spectra were recorded on different locations on the same sample to provide a consistent statistical evaluation. The spectral datasets were processed in Omnic software for polynomial baseline-correction. Concerning the EBS on HDPE spectra, Omnic peak area tool was used to calculate the band integrals under the NH stretching mode at 3300 cm^{-1}. For studying the relationship between spectral response and layer thicknesses, the band integrals calculated from both FTIR and Raman measurements were plotted against the respective stearamide layer thickness derived from XRF measurements. For IR datasets, a linear fitting routine in Origin 8G was applied for the band integral/layer thickness plot. For the Raman datasets, the applied fitting procedure was a weighted total least square (WTLS) regression, and was implemented by means of a MATLAB®-based tool for calibration [15] that is able to deal with uncertainty (and correlation) in both the dependent (average band integrals) and independent (thickness values) variables. The obtained calibration curves were used as the basis for subsequent quantitative analyses of EBS on hip liners. The uncertainty of the corresponding analysis curves was obtained by propagation of the probability distributions characterizing the calibration parameters and the band integrals at 3300 cm^{-1}, corresponding to the unknown thickness value, by applying a Monte Carlo simulation according to international guidelines [16].

Vibrational spectroscopic datasets from both FTIR and Raman spectroscopic techniques were exploited for 2D correlation analysis in the spectral region from 3400 cm^{-1} to 2800 cm^{-1}, and for FTIR data additionally in the spectral range between 1700 $cm^{-1}$and 1500 cm-1 applying the program *2Dshige v1.3* developed by Morita *et al.* [17].

For Raman experiments, layer thicknesses of 10 nm, 50 nm and 100 nm were considered, for IR additionally one further sample with a layer thickness of 600 nm was taken into account for spectral analysis.

Synchronous Φ correlation amplitudes were calculated from IR and Raman datasets, and plotted as $A(\nu_1)$ vs. $A(\nu_1)$ (auto-correlation), and with respect to IR and Raman spectra as $A(\nu_1)$ vs. $A(\nu_2)$ (cross-correlation). The calculation of the synchronous correlation amplitude Φ is described in the SM. The synchronous correlation amplitude Φ can be calculated according to the equation:

$$\Phi(\nu_1,\nu_2) = \frac{1}{m-1}\sum_{j=1}^{m} A_j(\nu_1)A_j(\nu_2) \ ,$$

$A_j(n_k)$ corresponds to the spectral absorbance with respect to the averaged (over parameter x) absorbance, from spectra within a certain data interval. 2D correlation allows for the study of systematic changes of the signal with respect to a "perturbation" such as increasing/decreasing peak intensities that are translated into constructing/deconstructing patterns at similar/dissimilar wavelength due to (i) T-induced changes (or pH, p, etc.) in molecular structure or (ii) due to modifications on chemical components that are mirrored in the spectral datasets.[18,19]

3. Results and discussion.

3.1. Analysis of 'model' stearamide contaminant layers on Si and HDPE substrates.

3.1.1. Chemical analysis of stearamide by XRF and NEXAFS.

The quantification of the model systems has been carried out by XRF. Exemplarily, Figure 2 shows XRF spectra recorded with an excitation energy of 1060 eV at an incidence angle of 45° for different layer thicknesses of stearamide on HDPE substrate with the expected fluorescence lines. Additionally, contaminations from elements such as F and Cu were identified. The respective calculated mass deposition and atoms per cm^2 for each model system are listed in Table 1.

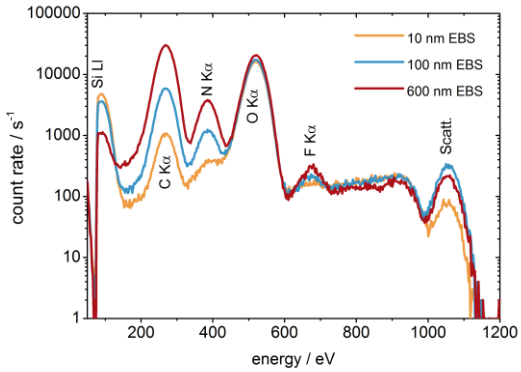

Figure 2. XRF spectra measured at 1060 eV at an incidence angle of 45° for the stearamide model system at nominally 10 nm, 50 nm, 100 nm, and 600 nm deposited on a silicon wafer.

For the determination of the layer thickness, a bulk density of 0.9 g/cm³ and only the N Kα fluorescence line was considered, assuming stoichiometric stearamide. Additional analysis of the N-K x-ray absorption edge confirms this course of action, as only the amide bond is observable and no other species are detectable.

In case of the deposition on Si, the mass depositions of C and O show that a reliable background subtraction of C and O is not possible. The oxygen contribution arising from the native oxide on the Si substrate was absorbed differently due to varying, and even unknown thicknesses of stearamide overlayers (especially for the thickest layer), and consequently was difficult to consider. Assuming stoichiometric stearamide and considering the N Kα fluorescence, one finds out that the calculated content of C is significantly different to the measured values (Table C1). The stearamide layers on HDPE show also an additional oxygen content which may originate from the substrate. Carbon was not considered either in that case, as it is also located in the HDPE substrate.

The thickness given in Table 1 confirms the nominal thickness of the 50 nm and 100 nm samples for both substrate types, but the samples with a nominal thickness of 600 nm are significantly thinner by about 360 nm. The nominally 10 nm stearamide layer on Si is three

times larger than expected, while the layers' thickness on HDPE substrate is in line with the nominal value.

Table 1. The mass depositions of C, N, and O with relative uncertainties of 15 % (k=1).

Mass deposition m/A µg/cm²				
Sample	Carbon	Nitrogen	Oxygen	Thickness d / nm
600 nm @ Si	29 ± 4	1.6 ± 0.2	0.51 ± 0.08	370 ± 60
100 nm @ Si	5.3 ± 0.8	0.48 ± 0.07	0.45 ± 0.07	112 ± 17
10 nm @ Si	0.87 ± 0.13	0.124 ± 0.019	0.26 ± 0.04	29 ± 4
600 nm @ HDPE	n.a	1.5 ± 0.2	2.0 ± 0.3	350 ± 50
100 nm @ HDPE	n.a	0.43 ±0.06	0.69 ± 0.10	101 ± 15
50 nm @ HDPE	n.a.	0.18 ± 0.03	0.33 ± 0.05	43 ± 6
10 nm @ HDPE	n.a.	0.056 ± 0.008	0.19 ± 0.02	13 ± 2

NEXAFS was employed to confirm the chemical binding state of the stearamide. In particular, the thickness determination of the stearamide layers relies on the nitrogen Kα fluorescence line. While the N-K NEXAFS spectrum exhibits only the specific run of the curve for stearamide and no further species contribution the calculation of the thickness provides reliable information. Otherwise the determined stearamide layer thickness is too large and a more elaborated procedure to separate the different species fraction would be needed. In addition to N-K absorption edge, the C-K and O-K near-edge region was measured for the model systems. In Figure 3 the spectra for the nominal 100 nm stearamide layer on Si substrate are shown for all relevant absorption edges. The C-K NEXAFS spectrum is characterized by two significant structures at 287.1 eV and 288.1 eV, which can be attributed to the C-H bond and the amide bond, respectively. The N-K NEXAFS spectrum is dominated by the amide π* at 401.1 eV followed by two broad structures being characteristic for the amide bond[20–22]. No further species containing nitrogen is observable. The O-K NEXAFS

spectrum also delineates structures being characteristic for amide bonds, but an additional species contribution exhibiting further peaks modifies the fine structure. In particular, the O-K NEXAFS spectrum of the nominal 10 nm thick stearamide layer indicates a second species which can be attributed to silicon dioxide that arises from the Si substrate. With an increasing stearamide layer thickness the influence almost vanishes, leading to a broadening of the stearamide fine structure. In case of the HDPE substrate, this behavior is not observable.

Organic compounds are sensitive to beam damage, in particular the amide bond [23–25]. The mechanism is well-known [25]. In our case, it has been considered that the amide bond may be modified during the measuring process in the way that a maximum dose has been experimentally determined. With this knowledge, the intensity of the beam was decreased that it could be excluded that the layers are modified during the analysis process. As shown in the report [25] the fine structure at the N-K x-ray absorption edge is significantly affected by a beam damage in a way that additional structures are observable.

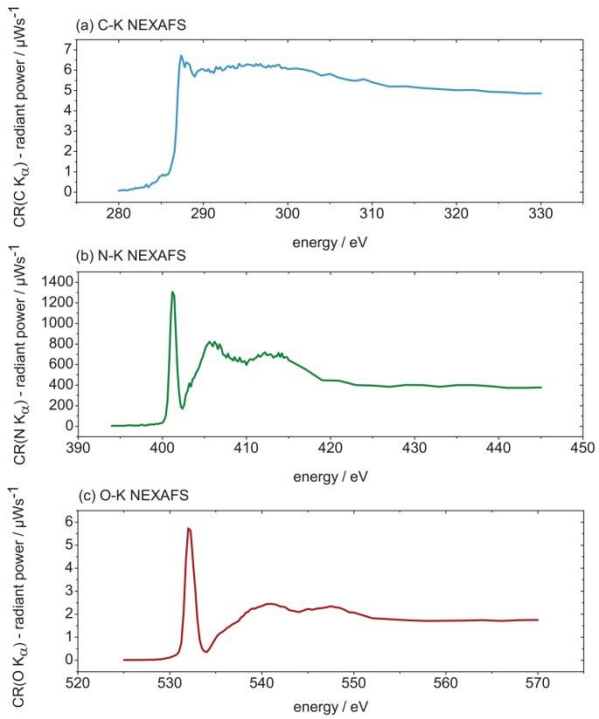

Figure 3. NEXAFS spectra of carbon (a), nitrogen (b), and oxygen (c) K x-ray absorption edges were measured for the nominally 100 nm thick EBS layer are shown exemplarily.

3.1.2. FTIR and Raman analyses.

Figure 4a displays the IR results. It is clearly observable that a decrease of intensity of the stearamide modes (gray marks) strongly correlates with a decrease of layer thicknesses. From univariate analysis we infer both IR and Raman typical modes originating from stearamide [26,27] (Table B1). Univariate analysis of IR data in the MIR spectral region delivered EBS typical modes that could be detected in the nominal layer thickness range, both on Si and HDPE substrates (Figure 4a). At about 1200 cm^{-1} a large dip can be noticed that derives from the crystalline silicon dioxide substrate background [28]. This background can be observed increasing, the thinner the layer coating becomes.

Raman signals of Si are mainly present in the region between 800 cm^{-1} to 1500 cm^{-1} of the spectrum where the 2nd, 3rd and 4th orders at 1000 cm^{-1}, 1450 cm^{-1} and 1940 cm^{-1}, are shown, respectively, (Figure 4b). Other signals related to the atmospheric oxygen and nitrogen N_2 are also present.

For the stearamide layers on Si we could identify three different spectral regions where layer thickness IR-sensitive modes occur: (i) at about 3300 cm^{-1} (ν – NH, ν – CH_2), (ii) 3300 cm^{-1} and 2900 cm^{-1} (ν – CH), and (iii) finally between 1700 $cm^{-1}$and 1500 cm^{-1} ν (C=O / C – N, C – C). For Raman, EBS-specific signals could be detected from 3500 cm^{-1} to 1600 cm^{-1}, revealing an increase with the respective stearamide thickness for the stretching vibrations of N-H and C=O groups at 3300 cm^{-1} and 1645 cm^{-1}, respectively, with no or minimal overlapping with the typical Si bands (Figure 4b) .

If we compare the results obtained from IR with those obtained by Raman spectroscopy we observe that of the region of CH_2 stretching modes is more or less insensitive towards EBS

layers being analyzed on HDPE. For IR data the amide II/I region seems to be the most sensitive spectral range with regard to the coating thicknesses on both substrate types.

Raman signals of the HDPE are mainly present in the spectral region from 3000 cm^{-1} to 2800 cm^{-1} and from 1500 cm^{-1} to 1300 cm^{-1} where the typical stretching and bending vibrations of the CH_x groups occur. Specific Raman signals of the stearamide cannot be observed in these spectral regions between 3000-2800 cm^{-1} and 1500-1400 cm^{-1} due to the strong contribution of the substrate. We conclude from this observation that CH_2 stretching modes originating from HDPE strongly overlap with the bands of the sample films, thus dominating the CH_2 features of EBS. A more clear identification of the EBS on the surface can be obtained in the spectral regions between 1700-1600 cm^{-1} and 3400-3250 cm^{-1} where the specific stretching vibrations of the C=O and the N-H groups are present. Since the N-H region at 3400-3250 cm^{-1} is free of any HDPE interference and the intensity of this signal increases proportionally with the thickness of the stearamide film, this region was selected for setting up calibration curves.

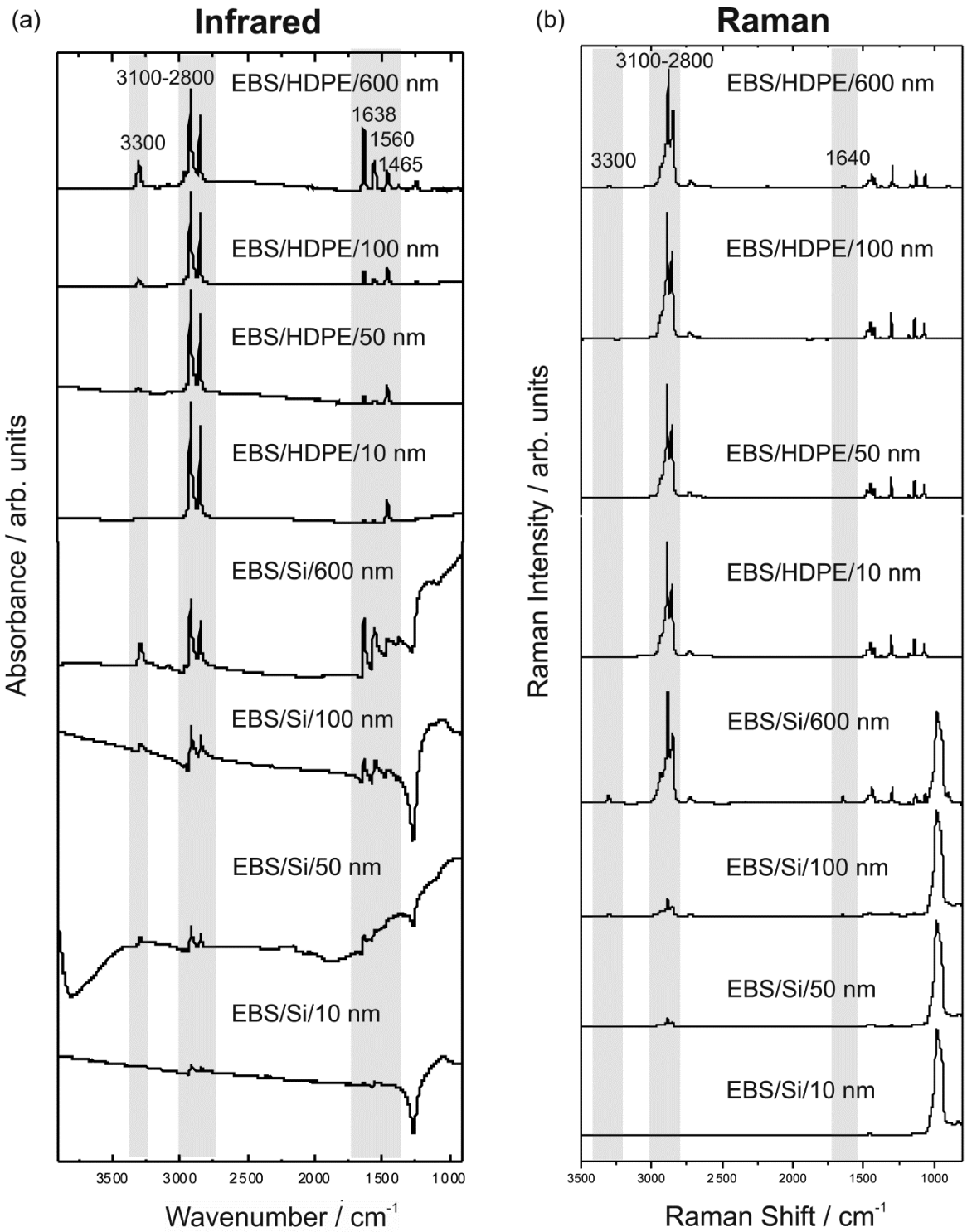

Figure 4. (a) MIR spectra of EBS on HDPE and Si with nominal layer thicknesses of 600 nm, 100 nm, 50 nm, and 10 nm, and (b) corresponding Raman data.

The 2D correlative analyzing tools in combination with indispensable ambient techniques such as IR and Raman spectroscopy provide further qualitative characterization opportunities of surface contaminants on in~/organic substrates. The layer thickness-sensitive modes unraveled by 2D correlation maps provide further information for a fast quantification of organic surface contaminants with the aim of a reliable identification in order to support the quality control of production-line biomedical devices.

The FTIR spectroscopical analysis was also supported by 2D correlative analysis, to which IR and Raman spectra could be entered. The use of this correlative tool enabled the study of complementary molecule-specific features of the different layer thicknesses as spectral changes in terms of intensity modifications could be assessed. Hence, 2D correlation was successfully exploited for visual decomposition of spectral complexity delivered by these complementary methodologies.

Three different spectral regions were identified where layer thickness-sensitive modes occur, for EBS layers on Si (and partially for EBS on HDPE substrates) for instance in the region between (i) 1700 cm^{-1} and 1500 cm^{-1} ν (C=O / C – N, C – C), (ii) 3300 cm^{-1} and 2900 cm^{-1} (ν – CH), and (iii) finally the region at about 3300 cm^{-1} (ν – NH, ν – CH_2). However, with respect to the analyses on HDPE (Figure 5 and Figure 6), from both IR and Raman experiments we could observe that the region of CH_2 stretching bands is insensitive towards contaminant layers. This is caused by CH_2 stretching modes originating from HDPE which strongly overlap with the bands of the sample film, thus dominating the CH_2 features of stearamide in this region.

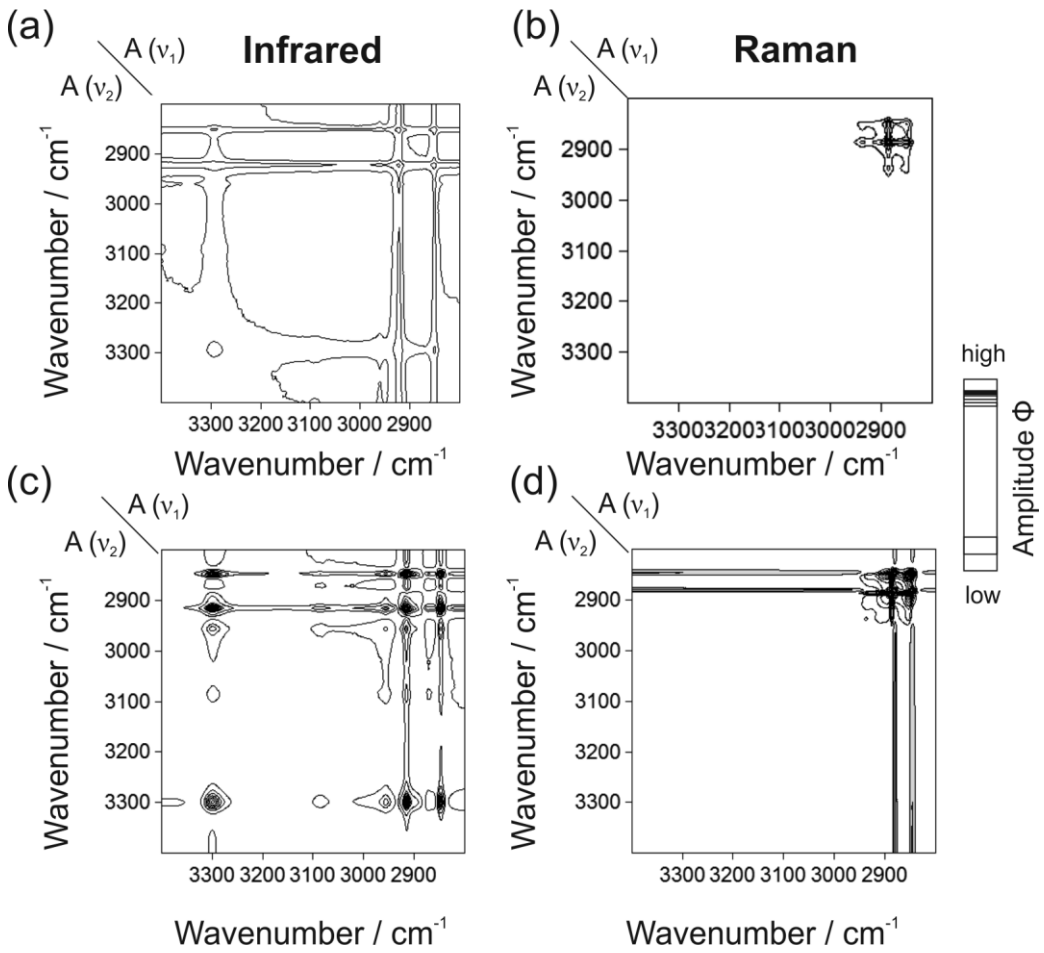

Figure 5. 2D correlograms of EBS sample films on Si: for (a) Infrared spectra of the nominally 10 nm, 50 nm, 100 nm, and 600 nm thick EBS films, and (b) Raman data of the nominally 10 nm, 50 nm, 100 nm, and 600 nm thick films. 2D correlograms of EBS films on HDPE for (c) Infrared data of nominally 10 nm, 50 nm, 100 nm, and 600 nm thick films, and for (d) Raman spectra of nominally 10 nm, 50 nm, 100 nm, and 600 nm thick films. Analysis was performed in the spectral range between 3400 cm^{-1} and 2800 cm^{-1}.

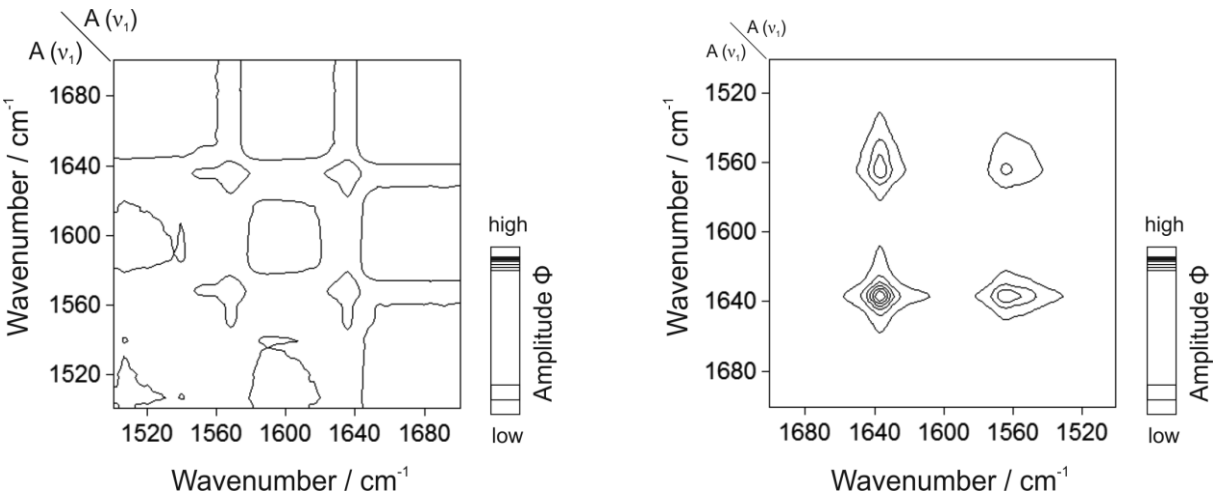

Figure 6. 2D correlogram of stearamide (10 nm, 50 nm, 100 nm, and 600 nm) on (a) Si and (b) on HDPE substrate. Analysis was performed in the spectral range between 1700 cm^{-1} and 1500 cm^{-1}.

3.2. Stearamide-coated 'real' biomedical devices – hip liners and wound dressings.

3.2.1. Chemical analysis by GIXRF and NEXAFS.

The analysis of medical devices is more challenging than for the model systems due to the unique surface structures and curvature. Figure 7 exhibits the spectra of one investigated hip liner and two wound dressings including a spectrum of an uncoated wound dressing as reference. The angle of incidence is characterized by an increased uncertainty in particular for the hip liner analysis. On basis of the calibration procedure developed for the model system with flat surfaces and a priori information about their nominal layer thicknesses, the hip liner and the wound dressings have been measured at a photon energy of 1060 eV and an incidence angle of 20°. The measured GIXRF spectrum of the hip liner is characterized by C-Kα, N-Kα, and O-Kα fluorescence lines. In addition, F-Kα, Cu-Lα, and Fe-Kα with low count rate can be observed which are attributed as surface contaminants on the hip liner. The spectra of the wound dressings are also characterized by the C-Kα, N-Kα, and O-Kα fluorescence lines.

Among these fluorescence lines Ag M lines are observable which originate from the coating of the polyurethane.

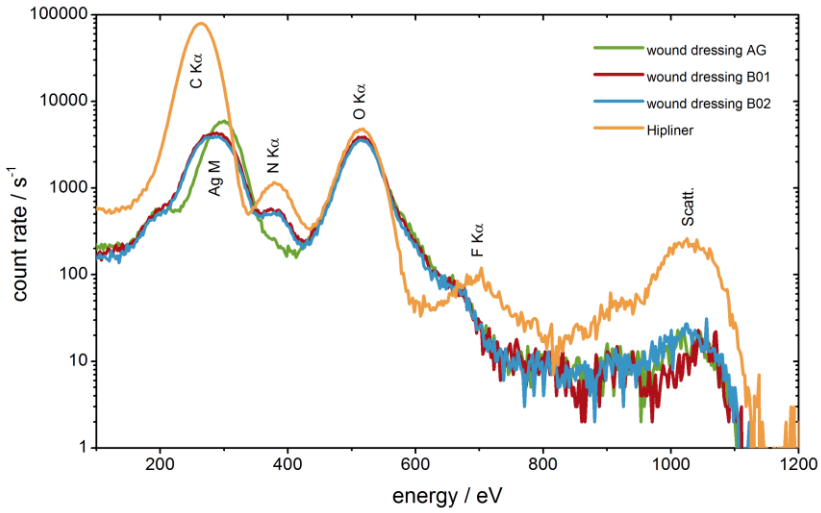

Figure 7. GIXRF spectra of a coated piece of hip liner and wound dressing AG – uncoated wound dressing, B01-02 stearamide coated wound dressing.

The mass deposition was determined by the reference-free GIXRF approach. For the determination of the thickness of the stearamide layer, only the N-Kα was considered due to that nitrogen is specific for stearamide. Assuming the bulk density of stearamide and known stoichiometry all other contributions can be concluded and finally a thickness for the stearamide layers. To confirm the stoichiometry of the stearamide again NEXAFS measurements were carried out showing spectra, which are typical for an amide bonding. This is as expected since other elemental contributions from C and O either contain unknown parts of contaminations or are dominated by the substrate.

The hip liner was measured on the center position including additional points close to the center, exhibiting thicknesses in the range of about 99 nm ± 15 nm. Complementary SIMS analysis shows a homogeneous layer thickness on the micrometer scale (cf. Appendix B). GIXRF results represent mean values due to the lateral resolution of about 500 µm × 20 µm. Furthermore, the GIXRF measurements are characterized by an increased oxygen content that

can be explained by a contamination of the surface of the hip liner. Measurements on the uncoated device show a significant oxygen contribution.

The two wound dressings were mapped on different positions exhibiting a homogeneous distribution of the stearamide. A mean thickness of the stearamide layer could be calculated for each sample: B01 exhibited a thickness of about 130 nm ± 20 nm and B02 of about 111 nm ± 17 nm. The Ag coating has the advantage that the signal from the polyurethane is almost suppressed for the GIXRF and NEXAFS analysis confirmed by measurements on the untreated sample. There are mainly Ag M lines observable, O-Kα from the AgO_x layer on top of the coating, and a small carbon contamination. Thereby, it turned out that the N-Kα fluorescence line is completely vanished. This is of importance, because polyurethane contains nitrogen bonded as amide and it would be indistinguishable to the stearamide. But, the Ag M lines are overlapping in parts C-Kα and N-Kα lines, respectively, and are hampering the de-convolution of the fluorescence spectra. In particular for the C-Kα, advance de-convolution strategies [29] are necessary knowing the transition probabilities of the respective Ag M fluorescence lines and a detector with better energy resolution. GIXRF measurements on the uncoated wound dressing are indicating that the Ag is in-homogeneously oxidized and the oxygen content is varying laterally. This makes a background subtraction difficult.

Additionally, the coated medical devices were analyzed by NEXAFS to validate the chemical binding state and to identify further contaminations. Both types of medical devices, hip liner and wound dressings, feature the typical resonances of stearamide. In contrast to that a further contribution cannot be observed at this edge.

In contrast to that, the analysis of the others x-ray absorption edges leads to a less significant result for the stearamide. In case of the wound dressings the oxygen K absorption edge shows the typical structure for stearamide, but additional resonances are observable which can be

attributed to silver oxide caused by the partially oxidized silver surface. As well as the measurements at the C-K absorption edge shows a fine structure that is specific for stearamide. The O-K NEXAFS spectrum of the hip liner shows contributions from the stearamide and contaminations.

3.2.2. FTIR- and Raman-based calibration curves and analyses of 'real' biomedical devices.

A linear correlation was found between the band integrals of the specific stearamide signals and the film-thicknesses since the chi-squared values (i.e. the sum of the weighted squared residuals normalized by the number of degrees of freedom) showed a high goodness of fit for both FTIR and Raman calibration curves, being close to the expected unit value (Figure 8a-b). The linear fit procedure was performed on the basis of band integral calculations of the NH stretching vibration of stearamide model contaminant layers on HDPE at 3300 cm^{-1}, the latter of which have been plotted over the layer thickness values originating from XRF analyses. In FTIR analysis, the band integral at 3300 cm^{-1} was afterwards determined for stearamide on the hip liner providing a stearamide layer thickness of 80 nm ± 17 nm for this biomedical device. The layer thicknesses were also evaluated for other band integrals at 1555 cm^{-1} and 1638 cm^{-1} for confirming the consistency. The thickness determined by the other band integrals is 120 nm ± 20 nm and 99 nm ± 18 nm, respectively, which is in the same order of magnitude. The slightly higher thickness can be explained by additional contributions from the substrate material. From FTIR investigations on EBS-coated wound dressings we could not receive any spectral feature that could be clearly assigned to EBS-specific modes, hence no band integrals could be calculated and used for the quantification implementing the constructed calibration curves based on stearamide model coatings.

Micro-Raman point mapping was performed on several locations on the surface of the device demonstrating its applicability even on substrates with a complex geometry. An uncoated hip liner was also measured as blank sample. The stearamide layer was successfully detected on the surface of the hip liner and an average spectrum was calculated from an area of about 1 cm^2 in order to provide a quantitative evaluation. Quantification of the stearamide was performed by using the calibration curve in Figure 8b and an average thickness of 102 nm ± 25 nm was calculated. The high uncertainty value was obtained due to the heterogeneous distribution of the EBS on the device which is more relevant if the characterization is performed with a technique at the sub-micrometric resolution. However, the present quantification is consistent with what was already reported by the other measurements.

Regarding Raman analysis on EBS-coated wound dressings, no signal related to the EBS was detected on it, which may be caused by the melting of the wound dressing supporting material, although using low laser powers and short integration times. We assumed that this effect was related to the presence of the silver on the wound dressing surface. Therefore, Raman spectroscopy demonstrated not to be suitable for the quantification of the EBS on these devices.

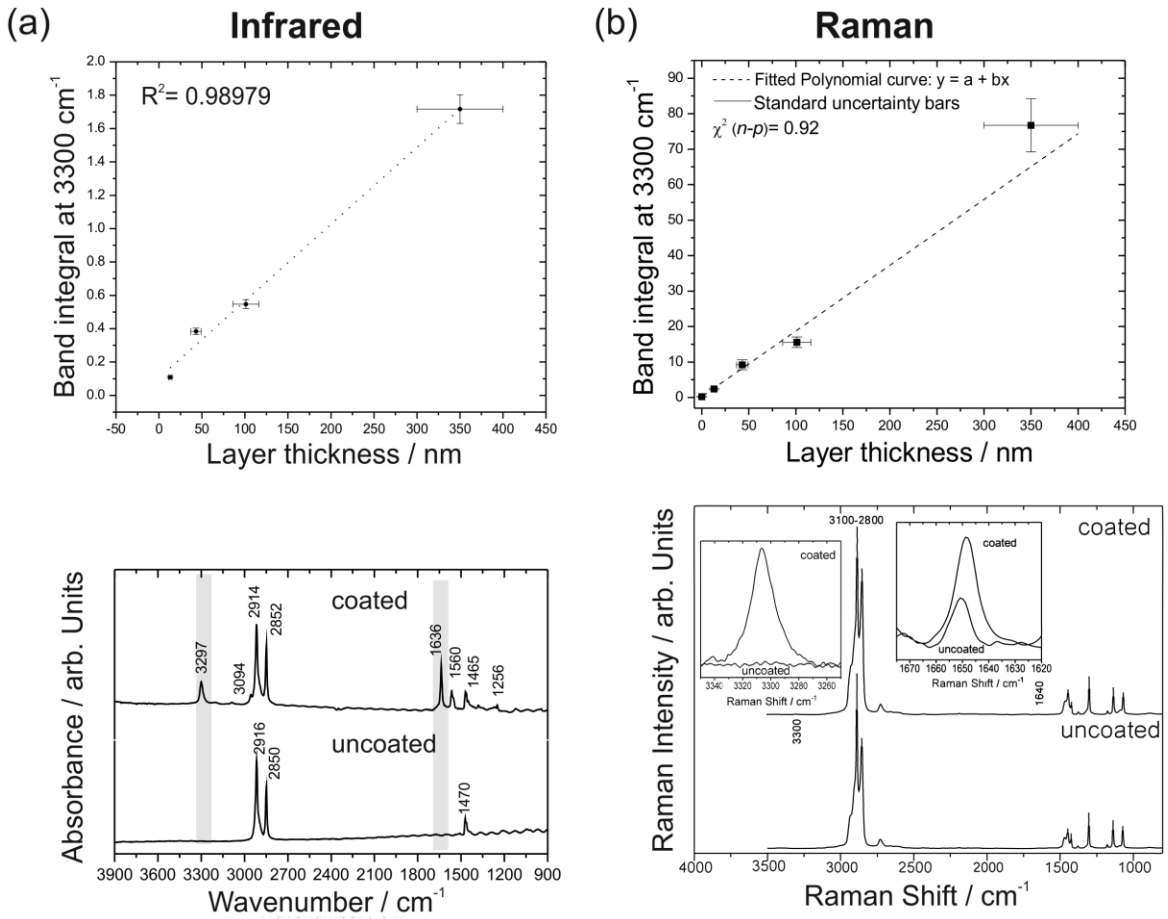

Figure 8. (a) Calibration curves constructed from the baseline-corrected band integral at 3300 cm^{-1} (black dotted lines), originating from FTIR data of the respective EBS model sample layer thickness (on HDPE. Error bars derive from the Gaussian fit procedures of 10 single FTIR spectra of the respective EBS layer thickness. **(b)** Calibration curve for the Raman datasets.

4. Conclusions.

Here, a calibration procedure has been successfully developed and validated by qualifying reference samples with different stearamide layer thicknesses on Si and HDPE, analyzed under implementation of different techniques such as XRF, FTIR, and Raman spectroscopy. The reference-free XRF serves as an absolute method allowing for the determination of mass deposition and thickness, if the density is known, hence providing traceability to the SI-based

unit kilogram [7]. FTIR and Raman spectroscopy, which are often available as bench top instrumentation in laboratories, enable the chemical speciation through the complementary identification of stearamide-specific modes and feature thickness-sensitive vibrational modes, which are differently pronounced for the respective method. Based on the XRF-results of the stearamide model samples calibration curves both for FTIR and Raman measurements could be ascertained, showing a linear connectivity with high regression coefficients.

To validate this procedure, real biomedical devices such as wound dressings and hip liners were dedicatedly contaminated with stearamide and analyzed by reference-free XRF, FTIR and Raman spectroscopy. The results have been thoroughly compared and discussed. In Table 2 a summary of the quantitative analysis of the stearamide coating on medical devices is presented. The results of the hip liner are coherent for FTIR, Raman spectroscopy, and GIXRF and do agree within the uncertainties. But for the wound dressing, Raman and FTIR spectroscopy could not detect any stearamide-related modes. Moreover, the laser used for Raman spectroscopy melted the substrate material.

This developed procedure can be used for the validation of calibration standards for advanced biomaterials, and the model systems presented here may be used as standards for FTIR and Raman bench top instrumentation. It clearly demonstrates the potential of combining complementary methods for a better understanding of complex organic-layered structures.

Table 2. Summary of quantitative analyses of stearamide coatings on biomedical devices.

Methodology	Medical device	Stearamide thickness / nm
XRF/NEXAFS	Wound dressing	STA1-B01 130 ± 20 STA1-B02 111 ± 17
	Hip liner	99 ± 15
FTIR	Wound dressing	n.a.
	Hip liner	80 ± 17
Raman	Wound dressing	n.a.
	Hip liner	102 ± 25

Acknowledgments.

We acknowledge financial support by the European Metrology Research Programme (EMRP). This work was funded through the EMRP Project IND56 Q-AIMDS. The EMRP is jointly funded by the EMRP participating countries within EURAMET and the European Union. The authors would like to thank Dr. Tara L. Salter for the preparation of the contaminated hip liners and wound dressings.

Appendix

A. Ellipsometry analysis on model EBS surface contaminants

Precise measurements of the stearamide coating thicknesses were made using a Woollam M-2000DI ellipsometer.. For ellipsometry measurements the film thickness can be delivered usually from optically flat, non-adsorbing surfaces, such as silicon. Ellipsometry of the silicon prior to evaporation and post evaporation was acquired from 65, 70 and 75 degrees and across a wavelength range of 500 to 1500 nm. The initial data was fitted using a silicon oxide on silicon model to determine the exact silicon dioxide thickness. Post evaporation a Cauchy layer was added to the model to account for the stearamide coating. By fitting the parameters of the Cauchy and to the ellipsometry data a film thickness could be determined. Values for the ellipsometry determined stearamide thickness across the range of samples are given in Table A1.

Table A1. ‘Model‘ biomedical devices and stearamide coating thicknesses. The thickness has been determined based on ellipsometry analysis on the coated Si wafers excluding the thickest samples.

Substrate	Stearamide coating	
	Nominal thickness / nm	Calibrated thickness / nm
Silicon	10	12.2 ± 1.8
Silicon	50	52.7 ± 3.5
Silicon	100	98.6 ± 4.2
Silicon	600	n.a.

B. Homogeneity studies of stearamide sample films by FTIR.

For homogeneity studies the model surface stearamide contaminant layers on Si (600 nm and 100 nm) were investigated, applying a grazing incidence (GIR) configuration combined with

the micro-spectroscopical FTIR setup which was equipped with a lN_2-cooled multi-element mercuric cadmium telluride detector, so-called focal plane array (FPA) detector with 128^2 pixel elements. MIR-signatures between 3900 cm^{-1} and 900 cm^{-1} were acquired with by co-adding 1064 scans at 4 cm^{-1} spectral resolution. The FPA experiments considered a sample region of 160^2 μm^2 that corresponds to 128^2 pixels (16,385 spectra), respectively.

The use of the Globar laboratory light source ensured a homogeneous illumination of a big sample surface area of 160^2 μm^2 that corresponded to 16,384 spectra.

For homogeneity studies, chemical maps for two layer thicknesses (600 nm and 100 nm) were constructed from GIR experimental datasets. The band integral of the mode at 1638 cm^{-1} was calculated and horizontal and vertical image pixel profiles were constructed through the middle of the chemical map, respectively.

Grazing incidence experiments on Si enabled the acquisition of FPA spectral datacubes for the construction of chemical images. From the images we both analysed horizontal and vertical image pixel profiles for studying the surface homogeneity of a 600 nm and 100 nm organic films. The chemical image analysis shows that both horizontal and vertical profiles deliver a constant color-coded intensity value with low intensity per pixel deviations (<5%), thus proving the homogenous constitution of the surface contaminant film.

The GIR experiments on Si enabled the acquisition of FPA spectral datacubes for the construction of chemical images in order to obtain a full picture of the micro-scaled area of the stearamide surface contaminants. Both vertical and horizontal pixel profiles illustrated a homogenous stearamide surface layer pattern. The calculated intensity profile highlights the intensity of the respective image pixel, the latter of which deviates not more than 2% from all other pixel intensities, no aggregates could be detected, thus proving the existence of a homogeneous surface layer coating. Concluding from these systematic FTIR analyses, their applicability as reference standards could be demonstrated.

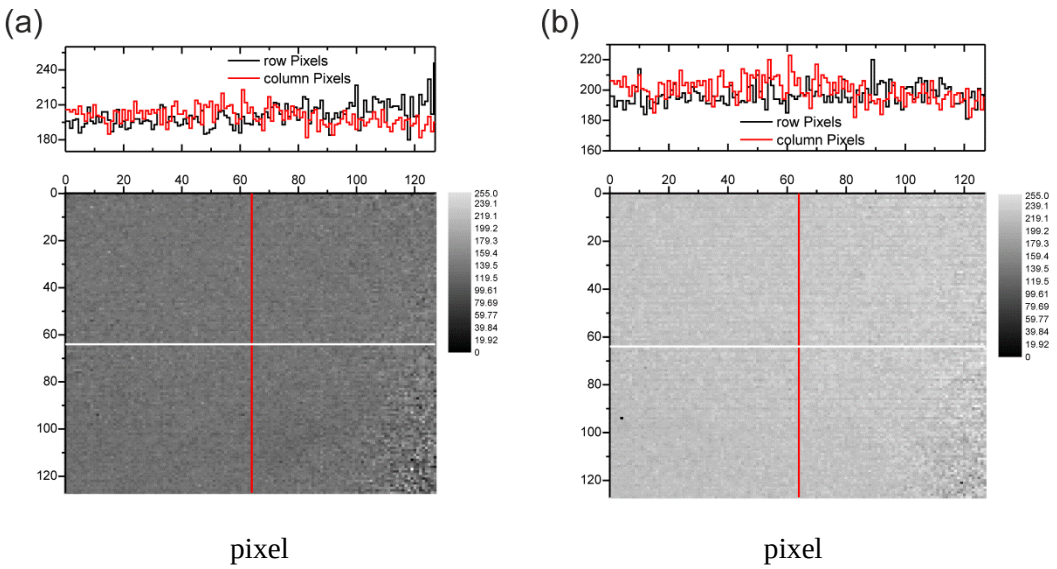

Figure B1. Chemical maps and image profiles of stearamide on Si with layer thicknesses of (a) 600 nm, and (b) 100 nm. For the images, the mode at 1638 cm^{-1} was calculated. Pixel size: 3 µm. Measurements were performed in grazing incidence configuration applying a Focal Plane Array (FPA, 15x IR) setup and a Globar light source.

Table B1. Tentative assignments of stearamide [30,31] sample films on Si and HDPE .

ν: stretching, δ: deformation (wagg.: wagging), ρ: rocking as: *asymmetrical*, s:*symmetrical*.[32–34].

*Modes of stearamide on HDPE, ** atmospheric N_2 or O_2, *** silicon, ****HDPE.

Mode / cm^{-1}	IR assignments	Mode / cm^{-1}	Raman assignments
3300	ν (N – H)	3300	ν (N – H)
2916	ν_{as} (–CH_2)	3000 – 2800****	$\nu_{as,s}$ (CH_x)
2840	ν_s (–CH_2)	2330**	N-N
1638	ν (C=O), δ (–NH_2)	1940***	4th order
1560	ν (C=O / C – N, C – C)	1645, 1650*	ν (C=O)

1465	δ (–CH_2)	1560**	O-O
1256	δ (C – H)	1550	ν (C-N)
725	δ (C – H), ν (N – H)	1400-1460****	$\delta_{as,\ s}$ (CH_2)
		1450***	3rd order
		1380****	δ (CH_3)
		1300 – 1100	ν (C-C)
		1297*, ****	$\delta_{wagg.}$ (CH_2)
		1170*, ****	ρ (CH_2)
		1131*,****	ν (C-C)
		1083****	ν (C-C)
		1064****	ν (C-C)
		1000***	2nd order

C. Quantitative XRF analysis.

Table C1. Considering the results on the N fluorescence and the stoichiometry of stearamide the mass deposition of C, O, and H have been calculated. The relative uncertainties are 15 % (k=1).

Mass deposition m/F µg/cm²

Sample	Carbon	Nitrogen	Oxygen	Hydrogen
600 nm @ Si	25.31	1.55	1.78	4.22
100 nm @ Si	7.78	0.48	0.55	1.30
10 nm @ Si	2.03	0.12	0.14	0.34
600 nm @ HDPE	24.47	1.50	1.72	4.08
100 nm @ HDPE	7.00	0.43	0.49	1.17
50 nm @ HDPE	2.99	0.18	0.21	0.50
10 nm @ HDPE	0.91	0.06	0.06	0.15

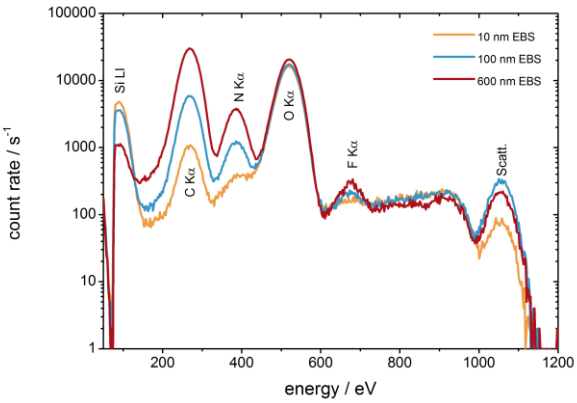

Figure C1. XRF spectra measured at 1060 eV at an incidence angle of 45° for the stearamide model system at nominally 10 nm, 50 nm, 100 nm, and 600 nm deposited on a silicon wafer. The fluorescence lines of the main material and substrate are clearly observable as well as contaminations such as fluorine and copper.

D. SIMS analysis of Stearamide coated medical devices.

SIMS analysis of polyethylene hip liner is shown Figure D1. and Figure D2. Figure D1 shows the SIMS mass spectra of a coated and uncoated hip liner. The marked peaks in Figure D1(b)

show the easily detected stearamide contamination seen from the second sample and is characteristic of the type of the ability of SIMS to detect levels of surface contamination.

Figure D2 shows images of a 250 by 250 μm area of a stearamide coated hip liner for (a) the total ion count and (b) the intensity of the stearamide characteristic peaks. Figure D2 shows up some interesting artifacts, from the hip liner with the ridges and curvature of the hip liner clearly observed to influence the ion intensities detected. Figure D2(b) shows a similar pattern of topography for the stearamide with an apparent even distribution across the surface. However due to these topographic effects it is difficult to qualitatively assess the evenness of the coating across the hip liner.

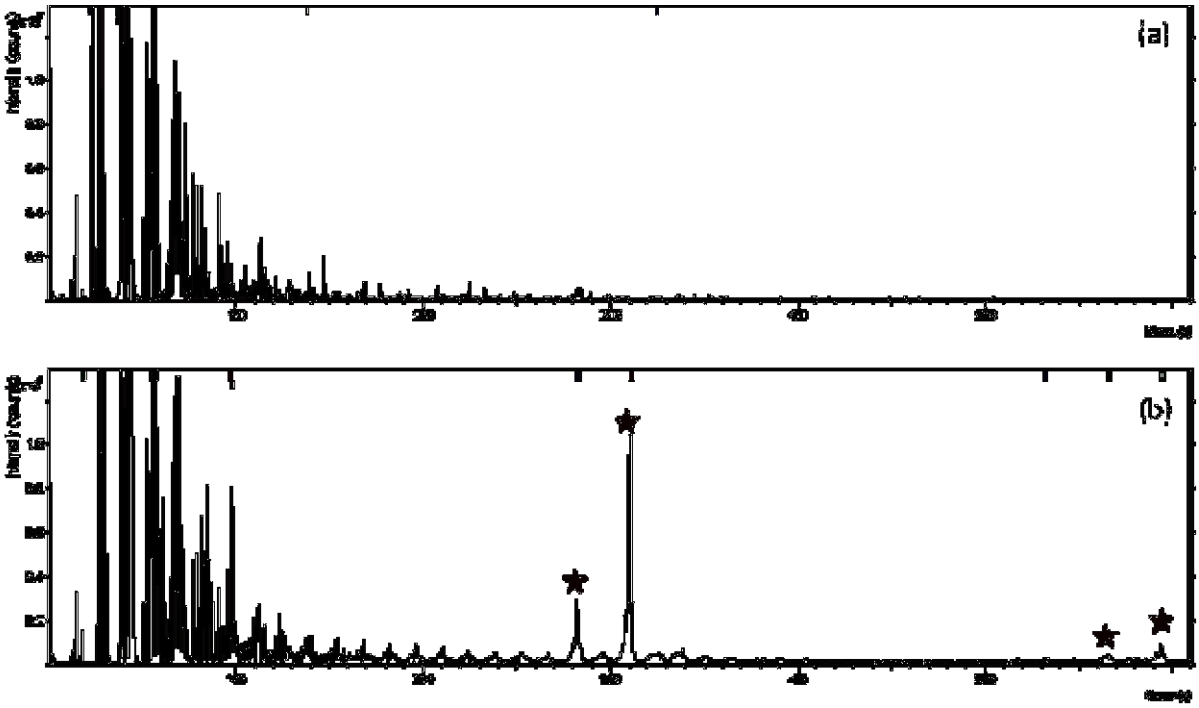

Figure D1. SIMS Mass spectra of (a) an uncoated hip liner and (b) a stearamide coated hip liner. Peaks characteristic for stearamide are marked with a star.

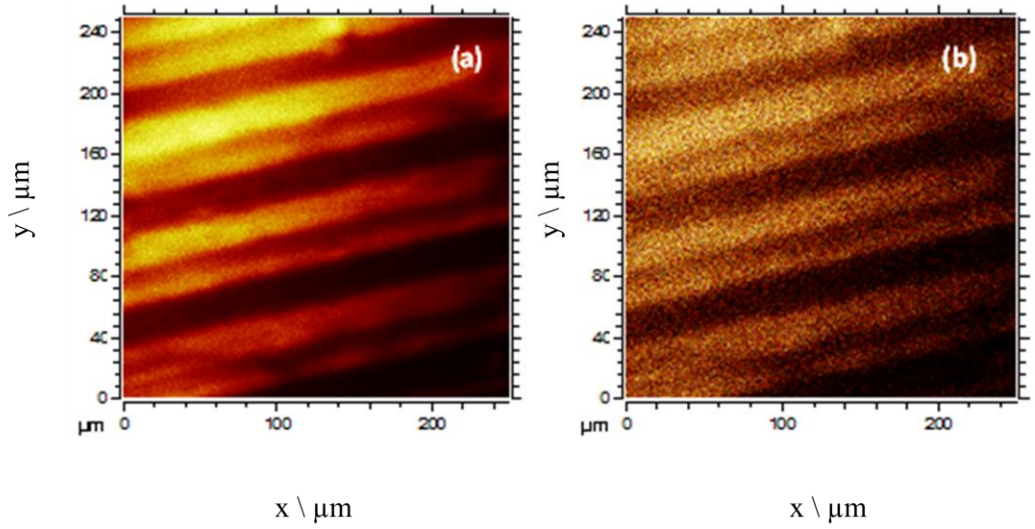

Figure D2. SIMS from a hip liner coated with stearamide. The image is of a 250 by 250 µm region with (a) total ion intensities and (b)) Stearamide ion intensities for the sum of the three molecular ions at 531, 565 and 593 Da and the fragment ion intensity at 310 Da, as labeled in the SIMS spectra in Figure D1(b) shown in the above image.

SIMS spectra of uncoated wound dressings show characteristic peaks of silver and a silane component, possibly PDMS. These signals are then almost completely masked by the stearamide coating on the contaminated surfaces indicating that coating is thick and largely intact. Figure D3 shows a 500 by 500 µm region of the Stearamide coating on the wound dressing. The representative stearamide ion intensity is shown in blue and is homogenously distributed across the surface with thin lines correspond to cracks in the coating where high levels of silver and PDMS ions (characteristic of the underlying wound dressing surface) are seen.

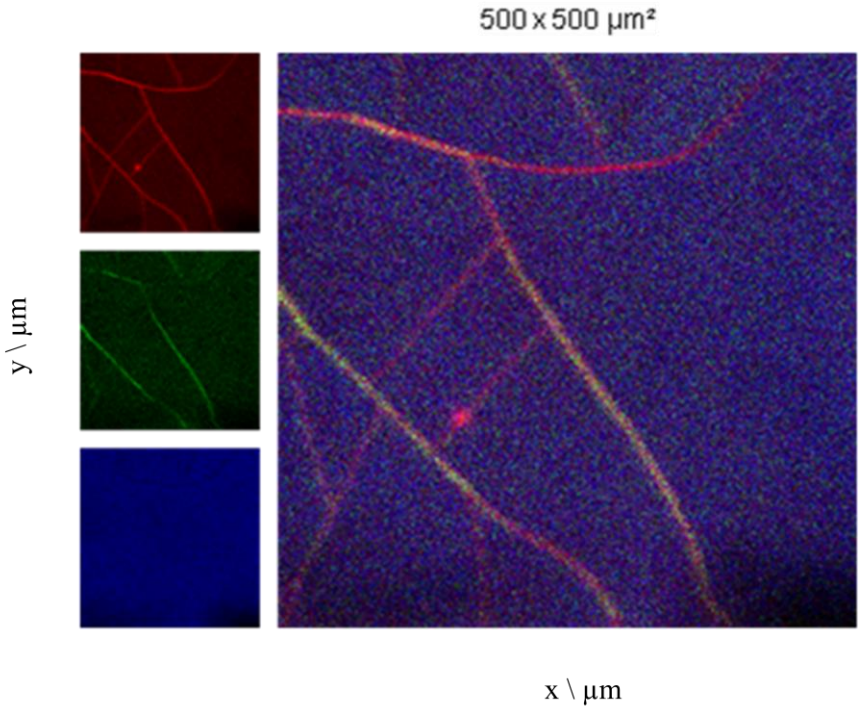

Figure D3. SIMS from a SMN wound dressing coated with Stearamide. The image is of a 500 by 500 µm region with intensities corresponding to PDMS (ion SiC3H9+), Ag ions and stearamide (molecular ion C20H40NO+) shown in red, green and blue respectively.

References.

[1] B.D. Ratner, Surface characterization of biomaterials by electron spectroscopy for chemical analysis., Ann. Biomed. Eng. 11 (1983) 313–36. doi:10.1007/BF02363290.

[2] B.D. Ratner, New ideas in biomaterials science-a path to engineered biomaterials, J. Biomed. Mater. Res. 27 (1993) 837–850.

[3] K. Andrascik, K-Andrascik, in: B.K. and E. Kanegsberg (Ed.), Handb. Crit. Clean., 2nd Applic, CRC Press, 2011: p. 574.

[4] B. Beckhoff, R. Fliegauf, M. Kolbe, M. Müller, J. Weser, G. Ulm, Reference-Free Total Reflection X-ray Fluorescence Analysis of Semiconductor Surfaces with Synchrotron Radiation, Anal. Chem. 79 (2007) 7873–7882. doi:10.1021/ac071236p.

[5] F. Senf, U. Flechsig, F. Eggenstein, W. Gudat, R. Klein, H. Rabus, G. Ulm, A plane-grating monochromator beamline for the PTB undulators at BESSY II, J. Synchrotron Rad. 5 (1998) 780–782.

[6] F. Scholze, B. Beckhoff, G. Brandt, R. Fliegauf, R. Klein, B. Meyer, D. Rost, D. Schmitz, M. Veldkamp, J. Weser, G. Ulm, E. Louis, A.E. Yakshin, S. Oestreich, F. Bijkerk, New PTB beamlines for high-accuracy EUV reflectometry at BESSY II, in: Proc. SPIE, 2000: p. 72.

[7] B. Beckhoff, Reference-free X-ray spectrometry based on metrology using synchrotron

radiation, J. Anal. At. Spectrom. 23 (2008) 845–853. doi:10.1039/B718355K.

[8] J. Lubeck, B. Beckhoff, R. Fliegauf, I. Holfelder, P. Hönicke, M. Müller, B. Pollakowski, F. Reinhardt, J. Weser, A novel instrument for quantitative nanoanalytics involving complementary X-ray methodologies, Rev. Sci. Instrum. 84 (2013). doi:http://dx.doi.org/10.1063/1.4798299.

[9] W.T. Elam, B.D. Ravel, J.R. Sieber, A new atomic database for X-ray spectroscopic calculations, Rad. Phys. Chem. 63 (2002) 121–128.

[10] H. Ebel, R. Svagera, M.F. Ebel, A. Shaltout, J.H. Hubbell, Numerical description of photoelectric absorption coefficients for fundamental parameter programs, X-Ray Spectrom. 32 (2003) 442–451.

[11] B. Beckhoff, G. Ulm, Determination of fluorescence yields using monochromized undulator radiation of high spectral purity and well known flux, Adv. X-Ray Anal. 44 (2001) 349–354.

[12] J. Feikes, M. Von Hartrott, M. Ries, P. Schmid, G. Wüstefeld, A. Hoehl, R. Klein, R. Müller, G. Ulm, Metrology Light Source: The first electron storage ring optimized for generating coherent THz radiation, Phys. Rev. Spec. Top. - Accel. Beams. 14 (2011). doi:10.1103/PhysRevSTAB.14.030705.

[13] R.M. and A.H. and A.M. and A.S. and G.U. and J.F. and M.R. and G. Wüstefeld, Status of the IR and THz beamlines at the Metrology Light Source, J. Phys. Conf. Ser. 359 (2012) 12004. http://stacks.iop.org/1742-6596/359/i=1/a=012004.

[14] R. Müller, A. Hoehl, R. Klein, A. Serdyukov, G. Ulm, J. Feikes, M. Von Hartrott, U. Schade, G. Wüstefeld, IR and THz beamlines at the metrology light source of the PTB, in: AIP Conf. Proc., 2010: pp. 32–35. doi:10.1063/1.3326341.

[15] A. Malengo, F. Pennecchi, A weighted total least-squares algorithm for any fitting model with correlated variables, Metrologia. 50 (2013) 654–662. doi:10.1088/0026-1394/50/6/654.

[16] Joint Committee for Guides in Metrology, Evaluation of measurement data — Supplement 1 to the “Guide to the expression of uncertainty in measurement” — Propagation of distributions using a Monte Carlo method, Evaluation. JCGM 101:2 (2008) 90.

[17] S.-I. Morita, Y. Ozaki, Pattern Recognitions of Band Shifting, Overlapping, and Broadening Using Global Phase Description Derived from Generalized Two-Dimensional Correlation Spectroscopy, Appl. Spectrosc. 56 (2002) 502–508. doi:10.1366/0003702021954953.

[18] I. Noda, Two-dimensional infrared spectroscopy, J. Am. Chem. Soc. 111 (1989) 8116–8118. doi:10.1021/ja00203a008.

[19] I. Noda, Two-Dimensional Infrared (2D IR) Spectroscopy: Theory and Applications, Appl. Spectrosc. 44 (1990) 550–561. doi:10.1366/0003702904087398.

[20] P. Leinweber, J. Kruse, F.L. Walley, A. Gillespie, K.-U. Eckhardt, R.I.R. Blythc, T. Regierc, Nitrogen K-edge XANES – an overview of reference compounds used to identify `unknown’ organic nitrogen in environmental samples, J. Synchrotron Rad. 14 (2007) 500–511. doi:10.1107/S0909049507042513.

[21] R. Giebler, B. Schulz, J. Reiche, L. Brehmer, M. Wühn, C. Wöll, A.P. Smith, S.G. Urquhart, H.W. Ade, W.E.S. Unger, Near-Edge X-ray Absorption Fine Structure Spectroscopy on Ordered Films of an Amphiphilic Derivate of 2,5-Diphenyl-1,3,4-Oxadiazole, Langmuir. 15 (1999) 1291–1298.

[22] A. Kade, D. V. Vyalikh, S. Danzenbächer, K. Kummer, A. Blüher, M. Mertig, A. Lanzara, A. Scholl, A. Doran, S.L. Molodtsov, X-ray Absorption Microscopy of Bacterial Surface Protein Layers: X-ray Damage, J. Phys. Chem. B. 111 (2007) 13491–13498. doi:10.1021/jp073650z.

[23] Y. Zubavichus, M. Zharnikov, A. Shaporenko, O. Fuchs, L. Weinhardt, C. Heske, E. Umbach, J.D. Denlinger, M. Grunze, Soft X-ray Induced Decomposition of Phenylalanine and Tyrosine: A Comparative Study, J. Phys. Chem. A. 108 (2004) 4557–4565.

[24] Y. Zubavichus, O. Fuchs, L. Weinhardt, C. Heske, E. Umbach, J.D. Denlinger, M. Grunze, Soft X-ray-induced decomposition of amino acids: an XPS, mass spectrometry, and NEXAFS study., Radiat. Res. 161 (2004) 346–358. doi:10.1667/RR3114.1.

[25] P.S. Johnson, P.L. Cook, X. Liu, W. Yang, Y. Bai, N.L. Abbott, F.J. Himpsel, Universal mechanism for breaking amide bonds by ionizing radiation, J. Chem. Phys. 135 (2011). doi:10.1063/1.3613638.

[26] H. Susi, Infrared Anisotropy and Structure of Crystalline Form C Stearic Acid and Vaccenic Acid2, J. Am. Chem. Soc. 81 (1959) 1535–1540. doi:10.1021/ja01516a004.

[27] K. Machida, S. Kojima, T. Uno, Infrared spectra of finite chain molecules—III, Spectrochim. Acta Part A Mol. Spectrosc. 28 (1972) 235–256. doi:10.1016/0584-8539(72)80249-6.

[28] P.J. Launer, Infrared Absorption Bands Characteristic of the Si-CH2CH2CN and Si-CH2CH2CH2CN Groups, Appl. Spectrosc. 22 (1968) 201–203. http://as.osa.org/abstract.cfm?URI=as-22-3-201 (accessed January 12, 2015).

[29] P. Hönicke, M. Kolbe, M. Müller, M. Mantler, M. Krämer, B. Beckhoff, Experimental verification of the individual energy dependencies of the partial L -shell photoionization cross sections of Pd and Mo, Phys. Rev. Lett. 113 (2014) 1–5. doi:10.1103/PhysRevLett.113.163001.

[30] G. Herzberg, Molecular spectra and molecular structure. I. Spectra of diatomic molecules., New York, 1950.

[31] F.T. FURUKAWA, S.H. SATO, Y. KITA, K. MATSUKAWA, H. YAMAGUCHI, S. OCHAI, H.W. SIESLER, Y. OZAKI, No TitleMolecular Structure, Crystallinity and Morphology of Polyethylene/Polypropylene Blends Studied by Raman Mapping, Scanning Electron Microscopy, Wide Angle X-Ray Diffraction, and Differential Scanning Calorimetry, Polym. J. 38 (2006) 1127.

[32] P.-A. Chollet, Infrared determination of the orientation of molecules in stearamide monolayers, J. Chem. Phys. 64 (1976) 1042. doi:10.1063/1.432313.

[33] W. Xu, M., Xu, M., Dai, H., Wang, S., and Wu, The Impact of Synthesis Conditions on the Structure and Properties of Di-(Stearylamidoethyl) Epoxypropyl Ammonium Chloride, Bioresources. 8 (2013) 3347–3357.

[34] F.S. Parker, Biochemical Applications of Infrared and Raman Spectroscopy, Appl. Spectrosc. 29 (1975) 129–147.